Molecular Therapy
Nucleic Acids
Original Article

Silencing of microRNA-106b-5p prevents doxorubicin-mediated cardiotoxicity through modulation of the PR55α/YY1/sST2 signaling axis

Antonio Lax,[1] Fernando Soler,[1] Maria Josefa Fernandez del Palacio,[2] Silvia Pascual-Oliver,[1] Miriam Ruiz Ballester,[1] Jose Javier Fuster,[3] Domingo Pascual-Figal,[3,4,5] and Maria del Carmen Asensio-Lopez[3]

[1]Biomedical Research Institute Virgen de la Arrixaca (IMIB-Arrixaca), University of Murcia, 30120 Murcia, Spain; [2]Veterinary Hospital, University of Murcia 30100 Murcia, Spain; [3]Centro Nacional de Investigaciones Cardiovasculares (CNIC), 28029 Madrid, Spain; [4]Cardiology Department, Hospital Virgen de la Arrixaca, IMIB-Arrixaca and University of Murcia, 30120 Murcia, Spain; [5]Centro de Investigación Biomédica en Red Enfermedades Cardiovasculares (CIBERCV), 28029 Madrid, Spain

Clinical use of doxorubicin (Dox), an anthracycline with potent anti-tumor effects, is limited because of its highly chemotherapy-induced cardiotoxicity (CIC). After myocardial infarction (MI), we have recently identified Yin Yang-1 (YY1) and histone deacetylase 4 (HDAC4) as two factors involved in the overexpression of the isoform soluble suppression of tumorigenicity 2 (sST2) protein, which acts as a decoy receptor blocking the favorable effects of IL-33. Therefore, high levels of sST2 are associated with increased fibrosis, remodeling, and worse cardiovascular outcomes. No data exist on the role of the YY1/HDAC4/sST2 axis in CIC. This study aimed to evaluate the pathophysiological implication of the molecular YY1/HDAC4/sST2 axis in remodeling that is developed in patients treated with Dox as well as to suggest a novel molecular therapy to prevent anthracycline-induced cardiotoxicity. Here, we have characterized a novel nexus between miR106b-5p (miR-106b) levels and the YY1/HDAC4 axis in relation to the cardiac expression of *sST2* using two experimental models with Dox-induced cardiotoxicity. The addition of Dox (5 μM) to human induced pluripotent stem cell-derived cardiomyocytes induced cellular apoptotic death via upregulation of *miR-106b-5p* (*miR-106b*), which was confirmed by specific mimic sequences. A functional blockage of miR-106b using the locked nucleic acid antagomir inhibited Dox-induced cardiotoxicity.

INTRODUCTION

Currently, half of all patients diagnosed with cancer will survive 10 years or more. This proportion approaches 75% for pediatric patients. This improvement in survival has made it possible to identify the cardiotoxic effect of cancer treatment including heart failure (HF).[1,2] Among anticancer drugs, anthracyclines are considered to be the main culprits of chemotherapy-induced cardiotoxicity (CIC), which can indeed affect the quality of life and survival, independently of the oncological prognosis.[3,4] Anthracycline-induced cardiotoxicity is a continuous and dose-dependent phenomenon that begins with damage at the cellular level of cardiomyocytes and may culminate in HF.[5,6] Current therapies have reduced the dose of anthracyclines but subclinical damage persists and can progress to HF, especially in patients with comorbidities. To date, there is no definitive and effective treatment to prevent anthracycline-induced cardiotoxicity. Indeed, these patients are treated similarly to non-oncologic patients.[7–9] Overall, these are suboptimal and non-specific treatments.

In the field of adverse remodeling after myocardial infarction (MI), our studies on the modulation of the poor prognostic suppression of tumorigenicity 2 (sST2) marker may have a profound impact on the management of patients with ischemic HF. In fact, to date, there is currently no treatment that is able to specifically lower sST2 levels. In a high percentage of patients, no matter what treatment they receive, their sST2 levels do not decrease at discharge. These patients have a poor prognosis and a higher index of death. Using computational genomics and an experimental animal model with ventricular dysfunction after MI, we have recently identified Yin Yang-1 (YY1) as a transcription factor able to activate *sST2* transcription in acute-phase HF. In addition, we characterized the molecular mechanism related to YY1 activation by establishing the role of the histone deacetylase 4 (HDAC4) as its necessary co-repressor.[10] Mechanistically, we revealed that the calcium/calmodulin-dependent protein kinase II-induced HDAC4 phosphorylation was able to prevent the import of HDAC4 from cytosol to the nucleus, which leads to activation of the YY1-induced *sST2* transcription, and a worse remodeling following MI.[10–12] Whether the YY1/HDAC4 axis is related to Dox-induced cardiac dysfunction in oncologic patients, the role of circulating sST2, and even the associated regulatory molecular mechanism, are unknown.

Received 15 September 2022; accepted 28 April 2023;
https://XXX

Correspondence: Antonio Lax, University of Murcia, Ctra. Madrid-Cartagena s/n, 30120 Murcia, Spain.
E-mail: alax@um.es
Correspondence: Maria del Carmen Asensio-López, Hematovascular Pathophysiology, Spanish National Center for Cardiovascular Research (CNIC), Madrid, Spain.
E-mail: mariadelcarmen.asensio@cnic.es

MicroRNAs (miRNAs) are small, non-coding RNA molecules that exert their regulatory function either by translational repression or by mRNA degradation of their targets.[13] In this study, we focused on *miRNA-106b-5p* (*miR-106b*) because of its known role in regulating cardiac processes in human and mouse disease models. miR-106b is included in the *miRNA106b-25* cluster[14,15] and, although its protective role in improving hypertrophy and cardiac function in left ventricular (LV) pressure overload and hypertrophy models has been reported,[16–18] it has also shown disparate results in other pathologies. In a study published in 2016, using an experimental animal model with cerebral ischemia/reperfusion injury, the authors demonstrated that its systemic silencing was able to ameliorate cerebral damage by blocking oxidative stress.[19] This is a pathological phenomenon that, according to other studies carried out recently, is activated by the sST2 protein.[20] Similarly, Rodriguez-Outeiriño et al. have recently suggested the use of antimiR-106b sequences as a treatment to increase muscle mass in injured Duchenne dystrophic muscle.[21] Regretfully, there is an understanding of whether there is a relationship between *miR-106b* and sST2 and even their relationship with anthracycline-induced cardiotoxicity, where oxidative stress plays a significant role.

In this study, we aimed to illuminate whether *miR-106b* is related to Dox-induced cardiotoxicity and evaluate the plausible implication of the YY1/HDAC4 axis and overexpression of *sST2* in the cardiac dysfunction induced by anthracycline. Our data demonstrate the role of the HDAC4/YY1 axis in Dox-induced cardiotoxicity and its molecular regulation by *miR-106b*, which leads to an increase in *sST2* expression and cardiac dysfunction. Functional and systemic *miR-106b* blocking before starting anthracycline treatment was able to prevent anthracycline-induced cardiotoxicity, which prevented the development of HF.

RESULTS

miR-106b-5p promotes Dox-induced apoptosis in iPSC-derived human cardiomyocytes

First, to evaluate whether *miR-106b-5p*, hereafter cited as *miR-106b*, takes part in the complex molecular mechanism involved in anthracycline-induced chronic HF, we assessed its modulation in human induced pluripotent stem cell (iPSC)-derived cardiomyocytes (hiPSCMs) exposed to 5 μM doxorubicin (Dox), a translational platform. Data analysis using quantitative real-time PCR revealed progressive upregulation of *miR-106b* levels following Dox treatment (Figure 1A). In particular, we evaluated a time-dependent increase in *miR-106b* levels, which was clearly visible after 3 h of treatment (2.3- ± 0.03-fold control; Figure 1A) and significantly higher after 15 h ($p < 0.001$). Furthermore, the *miR-106b* levels were progressively increased in the culture medium of hiPSCMs, being significant from 15 h of Dox treatment ($p < 0.001$) (Figure 1B). The results show that *miR-106b* levels are increased in hiPSCMs under Dox treatment. In addition, data analysis allowed us to select 15 h as the time of treatment with Dox for the following tests.

To validate the potential roles of *miR-106b* in Dox-induced cardiotoxicity, we next sought to inhibit miR-106b by using chemically modified antisense oligonucleotides. The efficiency of *miR-106b* inhibition was tested by assessing the expression level of a known *miR-106b* target, friend of GATA2 transcription cofactor (*FOG2*).[22] Compared with the antagomir negative control (AC), *antimiR-106b* (*AM106*) added in preincubation for 24 h was able to prevent the downregulation of *FOG2* mRNA levels when hiPSCMs were treated with Dox for 15 h (Figure S1A). Furthermore, AM106 treatment was able to prevent the release of lactate dehydrogenase (LDH, an enzyme increased in HF and tissue injury), the loss of Dox-induced cell viability, and significantly alleviate Dox-induced myocardial apoptosis, as documented by a decrease in caspase 3/7 activity (Figures 1C–1E). To demonstrate whether *miR-106b* participates in the regulation of the sensitivity of cardiomyocytes to Dox, a low dose of Dox (0.2 μM) was used to treat cardiomyocytes. Overexpression of *miR-106b* using an *miR-106b* mimic (*mimic-106b*) sensitized hiPSCMs to cell death in terms of a loss of cellular viability and an increase in caspase-3/7 activity (Figures 1F–1H). Taken together, our results suggest that human cardiomyocytes under Dox treatment can increase *miR-106b* levels, which is associated with Dox-induced cardiotoxicity *in vitro*.

PR55α is a downstream target of miR-106b

To explore the molecular mechanism by which *miR-106b* is involved in Dox-induced cardiotoxicity, we evaluated its potential targets using the bioinformatic programs *TargetScan*, *miRTarBase*, and *Enrichr*. We identified that the regulatory subunit of *PP2A* (protein phosphatase 2 regulatory subunit B isoform A serine/threonine-protein phosphatase 2A 55 kDa regulatory subunit B α isoform; *PR55α*) conserved binding sites for *miR-106b* (Figure 2A). Furthermore, we detected PR55α protein expression in the hiPSCMs upon Dox treatment and determined that PR55α protein expression was decreased in a time-dependent manner. As shown in Figure 2B, Dox treatment caused a decrease in PR55α protein levels, which was clearly visible after 6 h of treatment (2.6- ± 0.02-fold control) and significantly higher following 15 h ($p < 0.001$). A negative correlation was evaluated between *miR-106b* levels and PR55α protein levels in hiPSCMs treated with Dox ($r = -0.927$, $p < 0.001$) (Figure 2C). We then analyzed whether the decreased expression of PR55α protein was due to the increase of *miR-106b* after Dox treatment. We found that the inhibition of *miR-106b* recovered PR55α levels in hiPSCMs exposed to Dox treatment (Figure 2D). As shown in Figure 2E, the forced expression of *miR-106b* in hiPSCMs significantly attenuated PR55α levels. When we evaluated the effect of Dox treatment on PP2A activity (Figure 2F), data analysis showed that *AM106b* treatment prevented a Dox-induced PP2A activity decrease ($p < 0.001$), and the use of *mimic-106b* simulated the effect of Dox. Taken together, our results show that *miR-106b* could suppress PR55α protein levels in hiPSCMs under Dox treatment, which leads to a decrease in PP2A activity in hiPSCMs. Next, to demonstrate that *miR-106b* directly binds to the 3′ UTR of *PR55α* mRNA and downregulates PR55α protein synthesis, a luciferase gene reporter assay was used (Figures 2G–2I). We constructed two luciferase plasmids carrying a full-length *PR55α* (*Luc-PR55α-wt* [wild type]) and a mutated *PR55α* (*Luc-PR55α-mut*) (Figure 2G). Dual-luciferase reporter gene assay showed

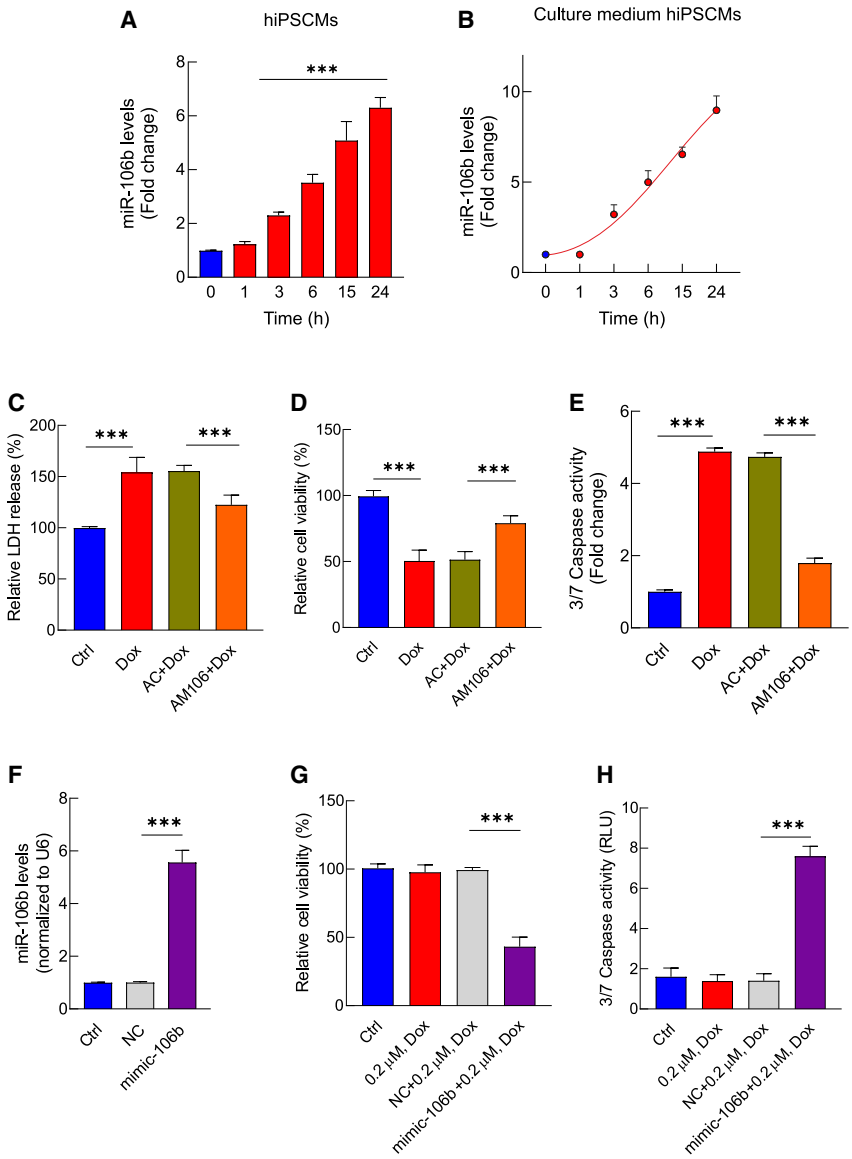

Figure 1. miR-106b promotes Dox-induced apoptosis in iPSC-derived human cardiomyocytes

miR-106b levels in hiPSCMs (A) and miR-106b levels in cell supernatant from hiPSCMs (B) normalized to U6. (C) LDH levels in cell supernatant obtained from hiPSCMs. (D) Relative cell viability. (E) Caspase-3/7 activity. (F) miR-106b levels. (G) Relative cell viability. (H) Caspase-3/7 activity. All quantifications are derived from n = 5 independent assays/group, and PCR experiments were performed with two replicates each. All quantitative data are presented as mean ± SEM. ***$p < 0.001$ determined by one-way ANOVA followed by post hoc tests with Bonferroni correction. U6, U6 small nucleolar RNA; Ctrl, control; AC, antimiR negative control; AM106, antimir-106b; and NC, negative control. Other abbreviations are described above.

that the relative activity of firefly luciferase of *Luc-PR55α-wt* in HEK293 cells was significantly decreased by the co-transfection of *miR-106b*, whereas it did not change the luciferase activity of *Luc-PR55α-mut* (Figures 2H–2I). Based on these findings, our data indicate that *PR55α* is a direct target of *miR-106b*.

miR-106b-induced PR55α downregulation favors cytosol accumulation of HDAC4 acting as a co-repressor of the YY1 transcription factor

Several studies have found that HDAC4 requires the actions of PP2A holoenzyme containing the PR55α subunit for its nuclear import and regulatory activity.[23,24] To test the effect of Dox on the HDAC4 levels, we first assessed whether Dox treatment was able to modulate the expression of *HDAC4* in hiPSCMs. Gene expression and protein levels of HDAC4 were analyzed by quantitative real-time PCR and western blot (Figure S2). Compared with the control group, Dox treatment resulted in a significant increase in *HDAC4* mRNA levels ($p < 0.001$), which was not prevented by *AM106b* (Figure S2A). These results were confirmed by assessing HDAC4 protein levels (Figure S2B). Then, to elucidate the role of HDAC4 in regulating YY1 activity, HDAC4 phosphorylation levels and HDAC4 subcellular distribution were studied using cytosolic and nuclear fractions from hiPSCMs under different experimental conditions (Figure 3). Western blotting analysis of cytoplasmic and nuclear protein extracts indicated that Dox treatment was able to increase the cytoplasmic accumulation of the phosphorylated HDAC4 protein ($p < 0.001$), which was prevented when human cardiomyocytes were pretreated with *AM106b* ($p < 0.001$) (Figures 3A–3C). As expected, a simulated overexpression of *miR-106b* by *mimic-106b* reproduced the effect of Dox ($p < 0.001$), with an increase of the cytoplasmic accumulation of phosphorylated HDAC4 form. Next, we tested whether *miR106b*-induced PR55α modulation may be related to the nucleus-cytoplasmic shuttling of HDAC4. Technically, we prevented *miR-106b*-induced *PR55α* downregulation by blocking the specific interaction site of *PR55α* for *miR-106b* with a miRNA target site blocker (*PR55α protector*). Our data reported that *PR55α protector* was able to prevent the Dox-induced cytoplasmic accumulation of phosphorylated HDAC4 form ($p < 0.001$) (Figures 3A–3C). The next step was to confirm the role of PR55α in the nucleus-cytosol shuttling of HDAC4, silencing *PR55α* expression. As shown in Figures 3A–3C, when hiPSCMs were co-transfected with *AM106* plus *PR55α* siRNA before Dox treatment for 24 h, *AM106* treatment was not able to prevent the Dox-induced increase of cytoplasmic accumulation of phosphorylated HDAC4 form. Finally, we tested the subcellular distribution of the total HDAC4 protein. Our data

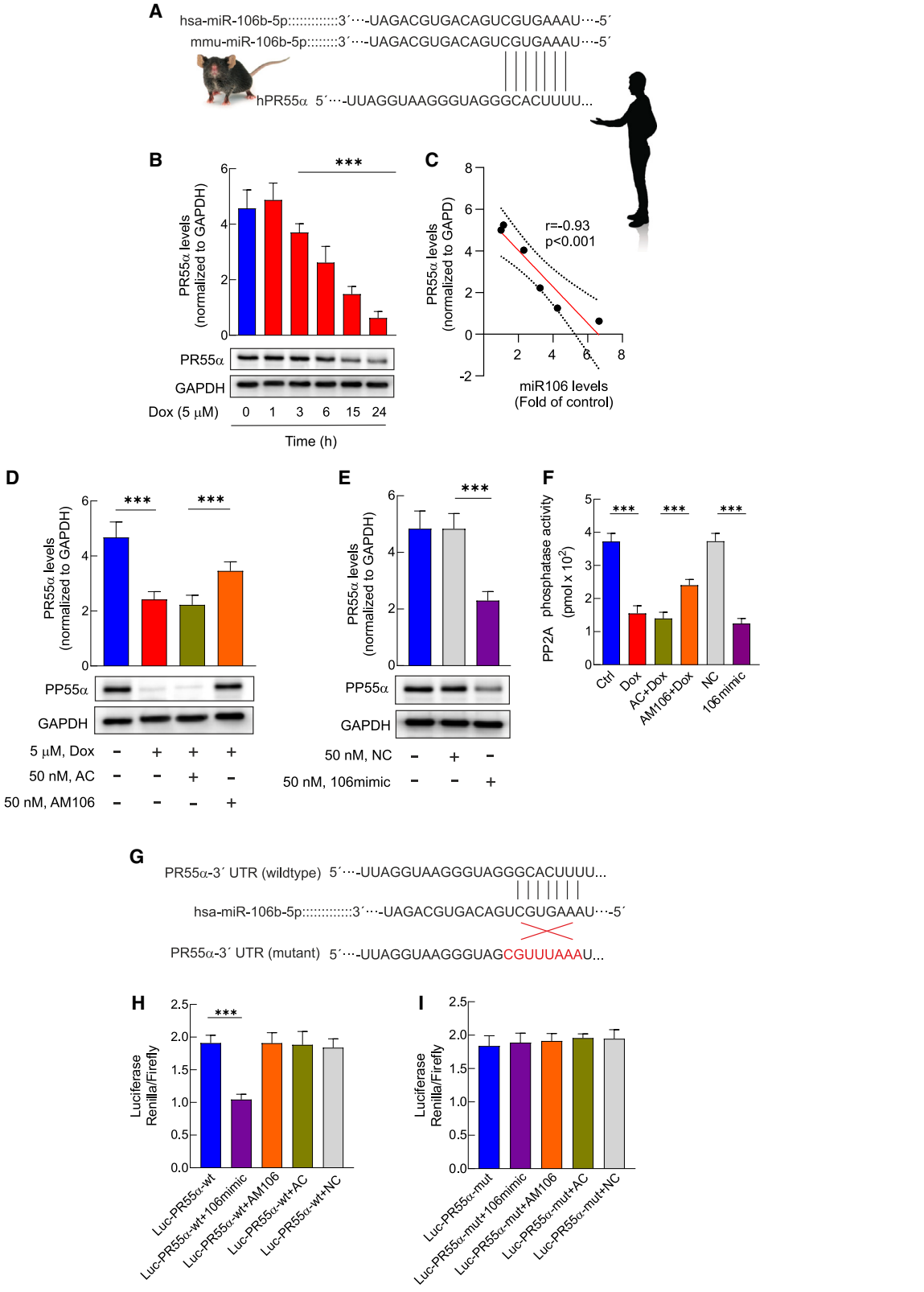

(legend on next page)

revealed that Dox was able to decrease the HDAC4 levels in the nuclear fraction ($p < 0.001$), which was prevented by *AM106* treatment ($p < 0.001$). As expected, the treatment with *mimic-106b* was able to decrease the accumulated levels of HDAC4 in the nuclear fraction ($p < 0.001$), and *PR55α protector* in combination with Dox significantly increased its nuclear level ($p < 0.001$). Moreover, co-transfection with *AM106* plus *PR55α* siRNA before Dox treatment was able to reduce HDAC4 levels ($p < 0.001$) in the nuclear fraction. Taken together, these results suggested that *miR-106b*-induced *PR55α* degradation was able to prevent the dephosphorylation of HDAC4, which leads to the accumulation of phosphorylated HDAC4 in the cytosolic fraction. It is important to note here that: (1) our data reported a nucleus-cytosol shuttling of the non-phosphorylated HDAC4 form favoring its accumulation in the cytosol in the context of injury with Dox and (2) when the total HDAC4 protein levels were tested without subcellular fractionation (Figure S2) a Dox-induced HDAC4 upregulation was revealed.

Once we identified that *PR55α* is a direct target of *miR-106b* and confirmed its relationship with HDAC4, the next step was to assess both the involvement of HDAC4 in anthracycline-induced cardiotoxicity as well as the molecular mechanisms implicated. Interactome analysis confirmed that HDAC4 was able to interact with the YY1 transcription factor in the human heart, with a score of 0.93 (Figure S3) (https://string-db.org/cgi/network?taskId=bhbQ5wIXQVyM&sessionId=bZ5SigiCT8v3). In this setting, the next step was to evaluate the effect of Dox on YY1 protein levels. When hiPSCMs were exposed to Dox for various prolonged periods, YY1 protein levels increased in a time-dependent manner, which was clearly visible after 6 h of treatment (3.8- ± 0.23-fold control; Figure 4A) and significantly higher following 15 h ($p < 0.001$). With the global aim of experimentally testing whether YY1 was able to interact with HDAC4, co-immunoprecipitation assays were carried out (Figure 4B–E). Initially, the nuclear fraction from hiPSCMs under different experimental conditions was co-immunoprecipitated with an HDAC4 antibody and probed with an anti-YY1 antibody. In parallel, the cited lysates were immunoprecipitated with an anti-YY1 antibody and probed with an anti-HDAC4 antibody (Figure 4B). This reciprocal co-immunoprecipitation experiment showed that Dox was able to prevent HDAC4-YY1 interaction, whereas *AM106* favored these interactions (Figures 4B–4D). Furthermore, overexpression of *miR-106b* using an *miR-106b* mimic simulated the effect of Dox, and the use of *PR55α protector* prevented *miR-106b*'s effect in the presence or absence of Dox (Figures 4B–4D).

Based on these and other results obtained previously by our research group using non-oncological experimental models with HF,[10] the next step was to study whether the cardioprotective effect attributed to *AM106* against Dox-induced cardiotoxicity was related to the modulation of the sST2 isoform (Figures 4F and S4) by the transcription factor YY1. In a first approach, an increase in sST2 protein levels was evaluated when hiPSCMs were exposed to Dox for 15 h (Figures 4F and S4A). As shown in Figure 4F, *AM106* treatment reversed this effect; *mimic-106b* simulated the effect of Dox and *PR55α protector* in the absence or presence of Dox decreased sST2 protein levels ($p < 0.001$ in all cases) (Figure 4F, left). Furthermore, the specific silencing of *PR55α* together with the functional blockade of *miR106b* (Figure 4F, right), or, conversely, the silencing of endogenous *YY1* expression (Figure S4A), allowed us to (1) characterize the involvement of the *miR106b/PR55α* axis in *sST2* expression and (2) evaluate the role of YY1 in *sST2* expression and its effect on cell viability. In this context, the silencing of *PR55α* reversed the effect of *AM106* on sST2 protein levels in Dox-treated hiPSCMs cells (Figure 4F, right) and the silencing of *YY1* prevented Dox from affecting sST2 protein levels (Figure S4A), which led to an improvement on the cell viability (Figure S4B). Taken together, our *in vitro* data suggested that Dox was able to increase sST2 protein levels through modulation of the *miR-106b*/HDAC4/YY1 axis and that this increase was related to anthracycline-induced cardiotoxicity.

Once we confirmed that Dox-induced sST2 protein overexpression in hiPSCMs was associated with a decrease in HDAC4-YY1 interaction and the role of *miR-106b*, the next step was to evaluate the implication of PR55α using a viral delivery strategy to overexpress hPR55α in hiPSCMs. First, the efficiency of transduction was tested by infecting hiPSCMs with *AAV6-EGFP* viral particles at an MOI of 10^4. After 7 days, more than 80% of the hiPSCMs expressed EGFP, as analyzed by immunostaining (data not shown). Following this, *AAV6-hPR55α* and *AAV6-empty* (*AAV6-Ctrl*) particles were produced to infect hiPSCMs again at an MOI of 1×10^4. The *AAV6-hPR55α* transduction resulted in a significant and stable induction of *hPR55α* mRNA expression in 7 days (Figure 4G). Dox strongly induced upregulation of sST2 protein levels in *AAV6-Ctrl*-treated cells, whereas cells treated with *AAV6-hPR55α* showed a significant decrease in sST2 levels (Figure 4H). To gain further insights into the role of sST2 in anthracycline-induced cardiotoxicity, we next examined whether incubation with the soluble extracellular domain of ST2 coupled with the Fc fragment of human IgG1 (sST2/Fc) could interfere with the cardioprotective effect of *AM106* treatment.

Figure 2. The PR55α regulatory subunit is a direct target of miR-106b

(A) Binding sequence of hsa-miR-106b and mmu-miR-106b within PR55α mRNA. (B) Representative western blot image and analysis of PR55α protein levels in cells treated with Dox for different time periods. (C) Correlation data between miR-106b vs. PR55α protein levels. (D and E) Representative western blot and analysis of PR55α protein levels in hiPSCMs subjected to different experimental treatments. (F) PP2A phosphatase activity in hiPSCMs subjected to different treatments. (G) Sequences and position of PR55α containing the wild-type and mutant binding sites of miR-106b that were cloned into the luciferase vector. (H and I) Luciferase assay. All quantifications are derived from n = 5 independent assays/group, PCR experiments were performed with two replicates each. All quantitative data are presented as mean ± SEM. ***$p < 0.001$ determined by one-way ANOVA followed by post hoc tests with Bonferroni correction. GAPDH, glyceraldehyde 3-phosphate dehydrogenase; Dox, doxorubicin. Other abbreviations have been described previously.

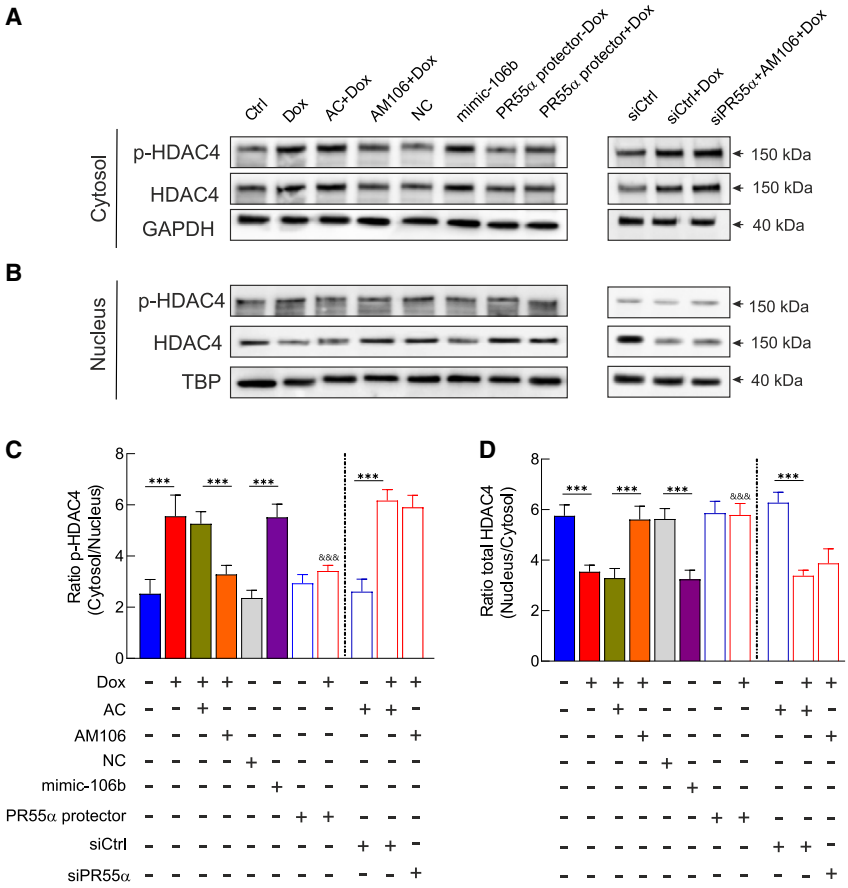

Figure 3. AntimiR-106b treatment prevents Dox-induced accumulation of phosphorylated HDAC4 in the cytosol

(A and B) Representative western blots of the levels of phosphorylated accumulation and total HDAC4 levels in cytosolic (A) and nuclear (B) extracts from hiPSCMs under different treatments. (C and D) Densitometric analysis calculated as the ratio of accumulated levels of phosphorylated HDAC4 in the cytosol to accumulated levels in the nucleus (C) and ratio of non-phosphorylated HDAC4 between the nucleus and cytosol (D). All quantifications are derived from n = 5 independent assays/group. All quantitative data are presented as mean ± SEM. ***p < 0.001 determined by one-way ANOVA followed by post hoc tests with Bonferroni correction. Abbreviations: TBP, TATA element-binding protein. Other abbreviations have been described previously.

As shown in Figure S5, exogenous sST2/Fc treatment was able to block the cardioprotective effect of *AM106* in terms of LDH release and cell viability ($p < 0.001$ in all cases).

AntimiR-106b treatment protects against Dox-induced cardiotoxicity *in vivo*

Once we identified the cardioprotective effect of *AM106* treatment against Dox-induced cardiotoxicity in a translational platform, the next step was to test whether this treatment was able to prevent Dox-induced cardiac dysfunction in an established experimental animal model. Based on our obtained *in vitro* results, we speculated that *in vivo* blocking of *miR-106b* could prevent the cardiotoxic effects of Dox by decreasing sST2 protein expression. Thus, to achieve a systemic loss of function of *miR-106b*, we injected *AM106* (20 mg/kg, i.v.) into mice 7 days before the first Dox injection (5 mg/kg, i.p.). Next, the mice were injected for 5 consecutive weeks, and simultaneously, with 5 mg/kg Dox and 20 mg/kg *AM106* and sacrificed 8 weeks later (Figure 5A). As shown in Figure 5B, and similarly to the data obtained for hiPSCMs, *miR106b* levels were evaluated as increased in LV myocardium from mice treated with Dox ($p < 0.001$). Furthermore, *AM106* treatment not only induced a significant upregulation of *FOG2* and *PR55α* mRNA levels in the presence of Dox ($p < 0.001$ in all cases) (Figures 5B and S1B, respectively) but it was also able to prevent Dox-induced cardiotoxicity. *AM106* treatment decreased both cardiac troponin T (c-TnT) levels and LDH activity as well as sST2 plasma levels ($p < 0.001$ in all cases) (Figure 5D). Furthermore, Dox treatment induced significant cardiac atrophy and fibrosis after the cumulative 25 mg/kg dose (Figure 5E). Importantly, the reductions in heart weight, cardiomyocyte size, and cardiac fibrosis were completely inhibited by pretreatment with *AM106* ($p < 0.001$ in all cases) (Figures 5F–5H). In addition, Dox showed a significant decline in ejection fraction (EF) and fractional shortening (FS), which were prevented by *AM106* treatment ($p < 0.001$ in both cases) (Figures 5I–5K and S6; Table 1).

Specifically, at 8 weeks of treatment, mice treated with Dox (Dox and AC + Dox groups) presented a significant reduction of several LV function parameters compared with the control group; that is, an increase of LVIDs and a decrease in SF, EF, CO, S′, and LV mass ($p < 0.001$ in all cases). However, neither the AC-treated Dox group nor the *AM106*-treated control group showed changes in systolic function when compared with their respective groups, Dox and control groups, respectively. On the contrary, the Dox group treated with *AM106* showed significant echocardiographic parameters characteristic of normal systolic function compared with the Dox group and the control group, indicating that *AM106* treatment was able to prevent Dox-induced systolic dysfunction. Similarly, mice treated with Dox plus *PR55α protector* showed LV echocardiographic parameters of systolic function not significantly different from the control group (Table 1). In addition, no significant differences were observed in the ratio of the early (E) to late (A) ventricular filling velocities (E/A) between the experimental groups. On the other hand, treatment with Dox was associated with a significant reduction of the mitral annular early diastolic velocity (E') and an increased E'/A′ ratio and E/A′ ratio

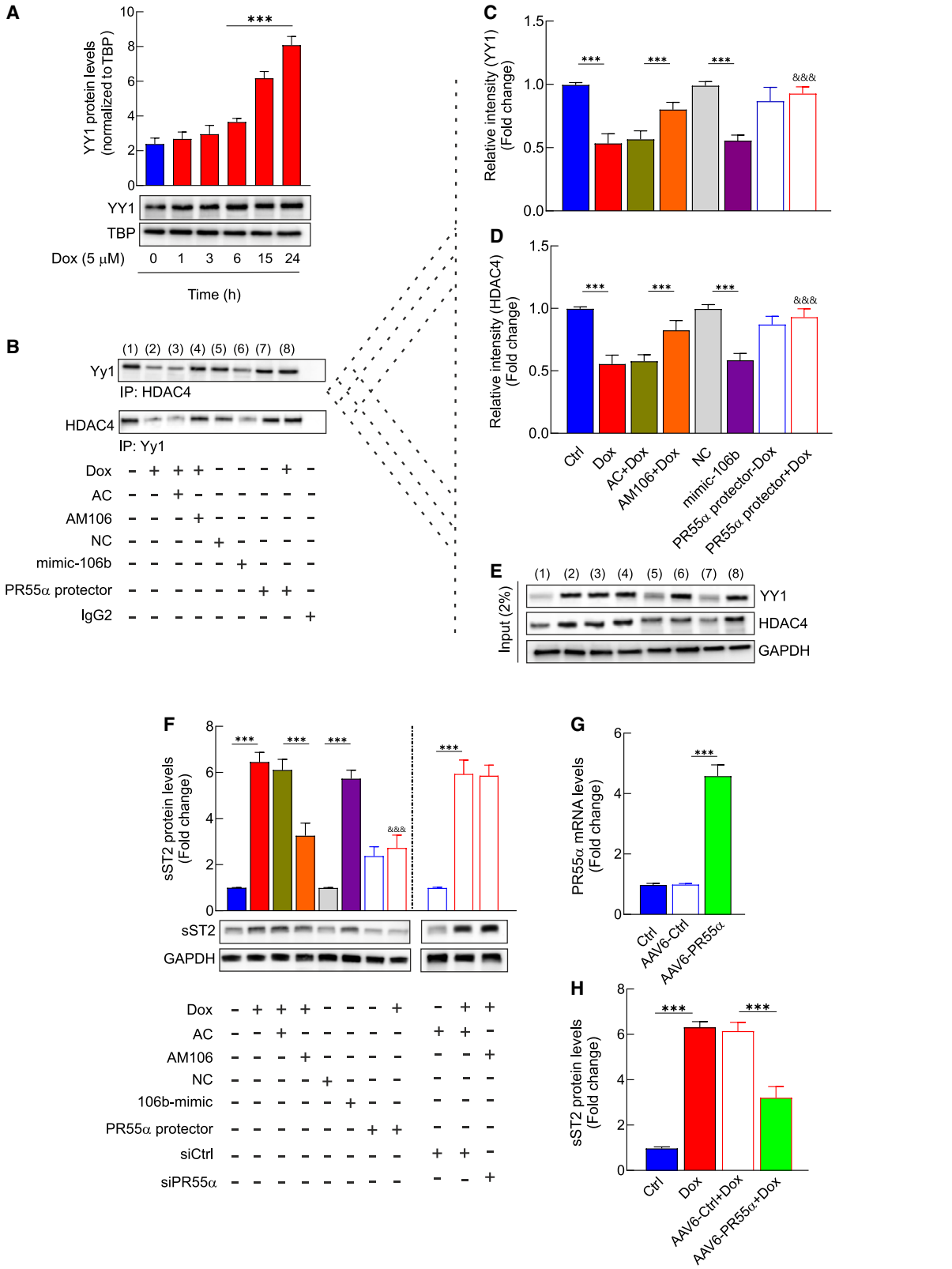

(legend on next page)

in relation to the control group at 8 weeks post-treatment. The Dox group treated with *AM106* showed no significant differences in relation to the control group, suggesting that treatment with *AM106* was able to prevent Dox-induced diastolic dysfunction. Likewise, mice treated with Dox plus *PR55α protector* showed echocardiographic parameters of diastolic function similar to the control group. In all cases, mice treated with *AM106b* showed no significant differences in relation to the control group (Table 1).

As expected, Dox treatment also induced cellular apoptosis, as detected by TUNEL staining and the activation of caspase-3/7 activity, which were prevented by *AM106* treatment ($p < 0.001$ in all cases) (Figures S7A–S7C). Dox treatment also resulted in whole-body cachexia, mainly due to reduced muscle mass, and *AM106* inhibited the loss of body mass ($p < 0.001$) (Figure S7D). Furthermore, *AM106* treatment was able to prevent the mortality associated with Dox treatment ($p < 0.001$) (Figure S7E).

Evaluation of the biodistribution and safety of AM106 treatment

As shown in Figure S8A, the *AM106b* was significantly increased in a time-dependent manner in LV myocardium at least up to the 6 days following *AM106* injection ($p < 0.001$ in all cases). *AM106* was also detected in the liver at (40.3% ± 7.2%), followed by the kidney (28.3% ± 6.2%), LV myocardium (22% ± 3%), and in a lower percentage in the lung (5.9% ± 0.5%) and spleen (3.5% ± 0.2%) throughout all 6 days in which the tissues were analyzed (Figure S8B). In addition, and as detailed in Figure S8C, control mice treated with *AM106* under the working plan detailed in Figure 5A and sacrificed after 8 weeks showed no pathological lesions in an organ other than the heart, which could be suggestive of toxicity or indirect-side effects. (Images of the AC-treated and saline groups are not included as they are similar to those of *AM106*.)

Downstream effectors of miR-106-5p

As expected, *AM106* treatment did not affect Dox-induced YY1 increase ($p < 0.001$) or Dox-induced HDAC4 increase (Figures 6A–6C) but prevented the effect of Dox on the YY1-HDAC4 interaction (Figures 6D–6F) ($p < 0.001$) in LV myocardium. Furthermore, mice treated with Dox showed higher HDAC4 total protein levels than control animals, which was not affected by *AM106* treatment (Figures 6G and 6H) ($p < 0.001$ in all cases). Again, mice treated with *PR55α protector* showed a similar response pattern to the use of *AM106* ($p < 0.001$) (Figures 6D–6I). Finally, to obtain more direct evidence that the beneficial effect of *AM106* treatment was related to the downregulation of myocardial *sST2* expression, we next examined whether the use of soluble sST2/Fc protein could interfere with the cardioprotective effect of *AM106* treatment. As shown in Figure 6J–6L, sST2/Fc treatment was able to prevent the cardioprotective effect of *AM106* in terms of c-TnT, LDH, and MDA levels ($p < 0.001$ in all cases).

Our results demonstrated that PR55α was highly involved in the *miR-106b*-dependent regulation of Dox-induced cardiotoxicity, and its degradation might be one of the mechanisms responsible for the loss of cardiac function, as seen in the case of the Dox-stress model applied. Noteworthy, we have demonstrated that Dox-induced *miR-106b* upregulation reduces cardiac PR55α levels, leading to the loss of PP2A phosphatase activity and accumulation of phosphorylated HDAC4 in the cytosol. Treatment with *AM106* prevents this signaling axis by favoring (1) the dephosphorylation of HDAC4 and its accumulation in the cell nucleus, (2) the interaction between HDAC4 and YY1 in the nucleus, and (3) the downregulation of the sST2 isoform.

DISCUSSION

In this study, we suggest a novel treatment to prevent CIC that develops in oncologic patients after receiving anthracycline-based chemotherapy. We provide the first evidence that links Dox-induced cardiotoxicity with an increase in both *miR-106b* levels and the cardiac sST2 isoform. Here, it was demonstrated that *miR-106b*-induced *PR55α* degradation leads to phosphorylated HDAC4 accumulation in the cytosol, activation of the YY1 transcription factor, and upregulation of the expression and release of the cardiac sST2 isoform. Interestingly, the combined use of Dox with *AM106* was able to decrease the myocardial sST2 isoform expression, which was associated with lower cardiac damage and, most importantly, a significant decrease in the mortality associated with chemotherapeutic treatment.

It is well documented that Dox is able to exert dose-dependent CIC in oncologic patients.[25] In fact, we found that mice exposed to Dox exhibited a loss in body and heart weight, increased cardiac apoptosis[26] and atrophy,[27,28] and, importantly, a decline in cardiac function, which led them to develop HF. Regrettably, it has to be highlighted that current therapies to prevent anthracycline-induced cardiotoxicity are suboptimal and non-specific. Consequently, the management of these patients is inadequate and, most importantly, the patients feel left alone and unprotected. Therefore, the search for a novel strategy able to counteract anthracycline-induced cardiac complications is extremely important, especially given the growing population of cancer survivors.[29] In this context, the involvement of miRNAs in almost all processes underlying cardiovascular disease raises the exciting possibility of therapeutic applications of these molecules.[30–32] Here, we

Figure 4. Anti-miR-106b treatment promotes HDAC4-YY1 interaction and prevents Dox-induced sST2 expression and secretion

(A) Representative western blot and analysis of YY1 protein levels in hiPSCMs subjected to Dox treatment for different time periods. (B–E) Reciprocal co-immunoprecipitation assays, representative western blot images, and HDAC4/YYY1 interaction analysis in nuclear fractions of hiPSCMs subjected to different treatments. (F) Representative western blot and analysis of sST2 protein levels in hiPSCMs under different treatments (normalized to GAPDH). (G) PR55α mRNA levels (normalized to GAPDH). (H) sST2 protein levels in supernatant obtained from hiPSCMs. All quantifications are derived from n = 5 independent assays/group, and PCR experiments were performed with two replicates each. All quantitative data are presented as mean ± SEM. ***$p < 0.001$ determined by one-way ANOVA followed by post hoc tests with Bonferroni correction. Abbreviations have been described previously.

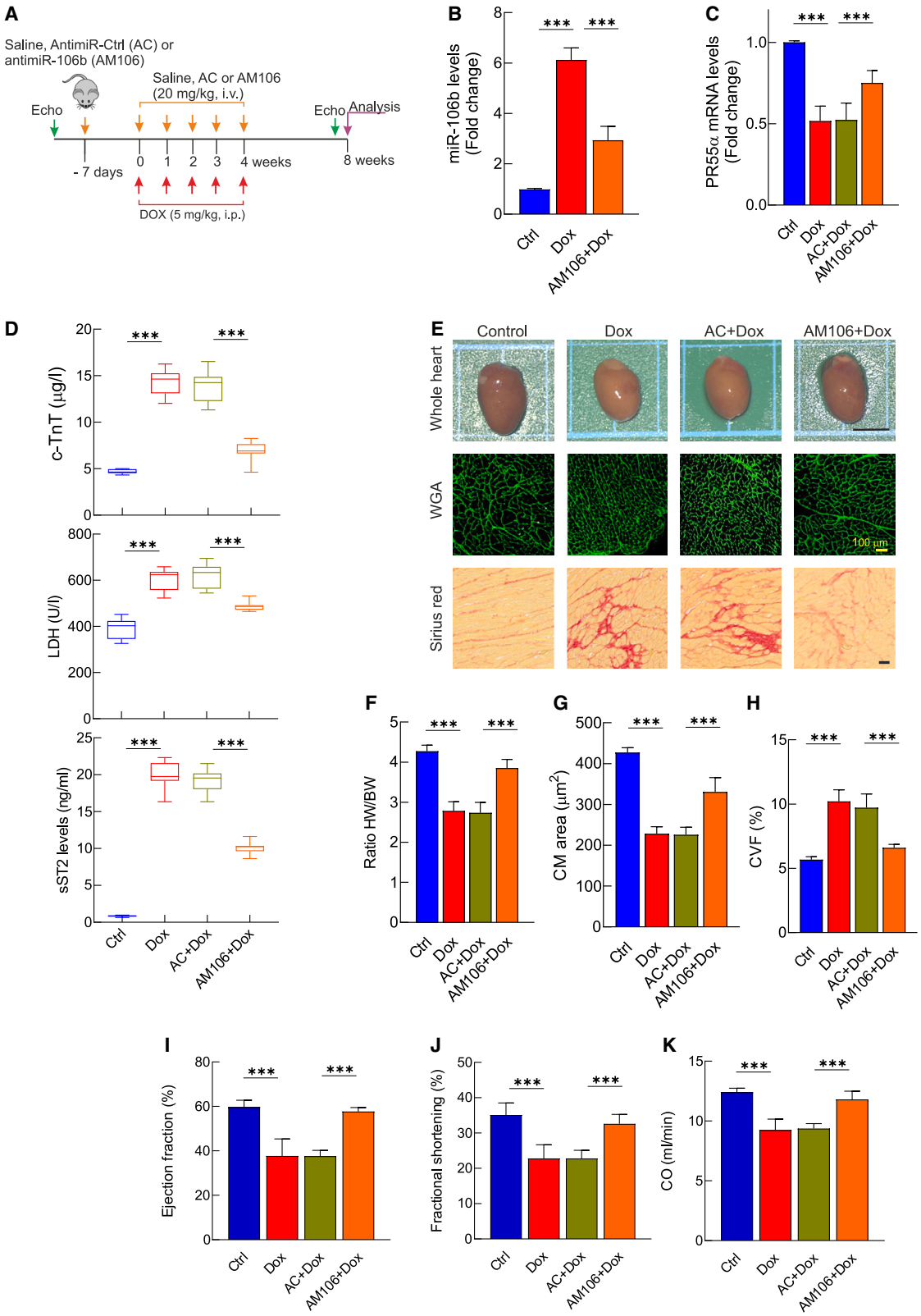

(legend on next page)

have focused our attention on the *miR-106b-93-25* cluster and revealed the key role of *miR-106b*, a miRNA that, despite being related to the development and pathophysiology of different types of cancer[33–35] and involved with oxidative damage and apoptotic cellular death,[19] has no studies evaluating its implication in Dox-induced cardiotoxicity. This is even more surprising when the relationship between oxidative damage, myocardial apoptosis, and anthracycline-induced cardiotoxicity is demonstrated.[26,36] The results of this study revealed a time-dependent increase of the *miR-106b* even after completing Dox treatment, which adds value to a previous study[37] and establishes its key role in the chronic-phase injury. In this scenario, it was tempting to speculate that *miR-106b* could be a possible mediator of the negative consequences driven by Dox; therefore, its functional blocking may have a cardioprotective effect. In fact, a systemic blocking of *miR-106b* was able not only to prevent the loss of muscle mass and cardiac atrophy associated with Dox treatment but also to induce: (1) an improvement in myocardial functionality, (2) a significant reduction in the mortality associated with chemotherapeutic treatment, and (3) an increase in the angiogenic capacity of myocardium injury. Indeed, in mice treated with Dox, echocardiographic parameters showed significant systolic and diastolic dysfunction as published previously,[38] which was prevented by *AM106b* treatment. Interestingly, these findings differ considerably from previous results reported in other research areas including hypertrophy-induced HF and LV pressure overload-induced HF.[39,40] Note that *miR-106* can bind to multiple targets and potentially be positive and negative gene expression regulators, which raises a dual role-dependent disease. In this context, while the cited studies revealed a protective role of *miR-106*, our data determine its deleterious function in the context of cancer treatment-induced cardiotoxicity. Indeed, our data are consistent with those of Li et al., who recently have revealed the cardioprotective role associated with the silencing of *miR-25*, a member of the *miR-106b-25* cluster, in an animal model of Dox-induced LV dysfunction.[37] In addition, this dual role of *miR-106b* was tested by evaluating the expression levels of *MFN2* and its relationship with cardiac hypertrophy. Although a link between *miR-106/MFN2* and hypertrophy has also been recently evaluated in models of HF with preserved EF (HFpEF), particularly in a murine model of thoracic aortic constriction-induced pressure overload[39] and in a hypertrophic murine HFpEF model,[40] our data revealed that Dox-induced *miR-106b* upregulation was associated with cardiac atrophy in parallel with a decrease of the MFN2 levels in LV myocardium from mice treated with Dox. These results are in agreement with several recently published studies evaluating the cardioprotective effect related to MFN2 as a potential strategy to mitigate Dox-induced cardiotoxicity.[41,42] In addition, the data presented here are also in good agreement with previous studies, which revealed that exposure to Dox prevented AngII-induced cardiac hypertrophy.[43,44] Indeed, our data reported a Dox-induced AngII upregulation, which did not induce hypertrophy. Although our study has not assessed the underlying mechanistic processes, the answer may lie in a study published by Xia et al., in 2020. The authors revealed that Dox-induced *FOXO1* upregulation in mice was able to block cardiomyocyte hypertrophy induced by multiple agonists, including AngII.[45]

Mechanistically, data analysis allowed us to identify a *miR-106b*-binding specific site in the 3′ UTR of the *PR55α* mRNA, a regulatory subunit of the serine/threonine PP2A phosphatase.[46,47] Due to its substrate spectrum, PP2A activity has a decisive influence not only on myocardial contractility but also on adverse cardiac remodeling.[48,49] In this setting, several studies have related a decrease in the expression of *PR55α* to abnormal PP2A activity and HF in non-oncological patients.[50,51] On the other hand, most reports of PP2A in the oncological area have shown it to be inhibited in human cancer, and its activation has shown promising therapeutic effects.[52] Therefore, it is tempting to speculate that the use of therapy targets directed at activating PP2A combined with anthracyclines could have a double benefit, increasing anti-tumor effects and preventing CIC. Understanding the molecular mechanisms that govern cardiac PP2A/PR55α activity and downstream molecular signaling is therefore desirable. A published work by Paroni et al. provided interesting findings about the relationship between PP2A/PR55α activity and HDAC4. The authors showed that HDAC4 requires the actions of the PP2A holoenzyme containing the PR55α regulatory subunit for its nuclear import.[23] Interestingly, and using a non-oncological experimental model with ischemic HF, our research group determined that this nuclear-cytosolic shuttling of HDAC4 is molecularly associated with cardiac dysfunction.[10] In that study, Asensio-Lopez et al. demonstrated that therapies targeting HDAC4 dephosphorylation led to its re-entering the nucleus, where it was able to act as a co-repressor of the YY1 transcription factor, leading to the downregulation of the circulating sST2 isoform and to improve cardiac remodeling after MI.[10] Here, we demonstrated that a Dox-induced *miR-106b* increase led to the accumulation of phosphorylated HDAC4 in the cytosol, losing its capacity to act as a genetic YY1 co-repressor, which was associated with sST2 protein expression and release. This is novel because this is the first study to characterize the role of the molecular HDAC4/YY1/sST2 axis with Dox-induced cardiotoxicity. Furthermore, our data suggested a relationship between cytosolic HDAC4 accumulation and a loss of PP2A activity

Figure 5. Anti-miR-106b treatment prevents Dox-induced cardiotoxicity in mice

(A) The design of the experimental study. Levels of miR-106b (normalized to U6) (B) and PR55α mRNA (normalized to GAPDH) (C) in LV myocardium. (D) Plasma levels of c-TnT, LDH, and sST2. (E) Upper panels: representative images of whole hearts under different treatments. Scale bar, 0.5 cm. Middle panels: micrographs obtained from left ventricles of mice subjected to different treatments and labeled with a WGA staining. Scale bar, 100 μm. Lower panels: micrographs obtained from left ventricles of mice subjected to different treatments and stained with Sirius red. Scale bar, 100 μm. (F) Ratio of heart weight to animal weight. (G) Cardiomyocyte area measurement. (H) Cardiac fibrotic area volume. (I–K) Representative cardiac function values were obtained using endpoint echocardiography. All quantifications were derived from n = 10 mice/group, and PCR experiments were performed with two replicates each. All quantitative data are presented as mean ± SEM. ***$p < 0.001$ determined by one-way ANOVA followed by post hoc tests with Bonferroni correction. LDH, lactate dehydrogenase; Echo, echocardiography. Other abbreviations have been described previously.

Table 1. Echocardiographic parameters for cardiac functions

Variable	Control	Dox	AC + Dox	AM106 + Dox	Control + AM106	PR55a + Dox
HR (beats/min)	453 ± 25	468 ± 20	565 ± 15	465 ± 21	451 ± 34	432 ± 21
LVDs (mm)	2.1 ± 0.2	2.9 ± 03*	2.9 ± 0.4	2.2 ± 0.1**	2.1 ± 0.2	2.2 ± 0.4
SF (%)	35 ± 5	21 ± 4*	20 ± 3	33 ± 6**	34 ± 6	35 ± 4
IVSs (mm)	1.5 ± 0.5	1.1 ± 0.1*	1.2 ± 0.2	1.5 ± 0.4**	1.5 ± 0.4	1.4 ± 0.4
LVPWs (mm)	1.4 ± 0.5	1.2 ± 0.2*	1.1 ± 0.1	1.4 ± 0.3**	1.5 ± 0.3	1.5 ± 0.4
LV mass (mg)	120 ± 14	79 ± 14*	84 ± 11	114 ± 12**	125 ± 15	121 ± 13
EF (%)	65 ± 9	37 ± 4*	41 ± 5	58 ± 4**	64 ± 4	62 ± 6
CO (mL/min)	13 ± 2	8.0 ± 2*	7 ± 2	12 ± 4**	14 ± 3	12 ± 4
S′ (mm/s)	21.4 ± 1.1	16.5 ± 0.9*	16.2 ± 0.5	22.7 ± 0.6**	20.4 ± 0.4	21.1 ± 0.3
E′ (mm/s)	23.3 ± 1.1	14.8 ± 0.5*	13.4 ± 0.8	24.4 ± 1.0**	23.5 ± 0.6	22.4 ± 0.5
A′ (mm/s)	19.3 ± 0.9	16.6 ± 1.5	17.6 ± 1.7	19.9 ± 0.8	18.5 ± 0.4	18.3 ± 1.2
E′/A′	1,25 ± 0.13	0,93 ± 0.06*	0,82 ± 0.08	1,24 ± 0.07**	1.24 ± 0.06	1,26 ± 0.05
E/E′	29.4 ± 2.6	59.8 ± 1.9*	66.12 ± 5.9	28.4 ± 1.4**	27.5 ± 1.2	28.5 ± 2.3
E/A	1.7 ± 0.16	1.7 ± 0.06	1.7 ± 0.15	1.6 ± 0.04	1.8 ± 0.04	1.6 ± 0.03

HR, heart rate; LV, left ventricle; LVDs, left ventricular systolic dimensions; SF, shortening fraction; IVSs, interventricular septal systolic thicknesses; LVPWs, left ventricular free wall systolic thicknesses; EF, ejection fraction; CO, cardiac output; E, early diastolic peak velocity of mitral valve flow; A, late diastolic peak velocity of mitral valve flow; S′, peak systolic; E′, early diastolic velocity of medial mitral annulus; A′, late diastolic velocity of medial mitral annulus. Data are expressed as mean ± SEM.
*$p < 0.05$ vs. control and Dox groups; **$p < 0.05$ vs. Dox + AM106 and DOX + AC groups.

due to the decreased expression of PR55α by *miR-106b*. This functional role was confirmed using different experimental strategies. First, *AM106* treatment prevented Dox-induced *PR55α* degradation, which led to PP2A activation and a decrease in the phosphorylation state of HDAC4 on its activating site Ser^{246}. These results were confirmed by overexpressing *miR-106b* levels or using specific sequences to block the interaction site of miR-106b on PR55α. It is important to note that, under our experimental conditions, HDAC4 was not a direct target of miR-106b because: (1) Dox was able to increase the HDAC4 levels in total protein fraction without prior subcellular fractionation and (2) *AM106b* treatment had no effect on Dox-induced HDAC4 upregulation in total protein fraction. According to the studies published by Guan et al.,[39] and later by Gallicano et al.,[40] these findings reported again the dual role of *miR-106* depending on the context of injury. While the cited studies show a direct relationship between *miR106* levels and hypertrophy, our data revealed different results under anthracycline-induced cardiotoxicity, which adds value to the fact of its dual role in relation to the context of the damage.

Furthermore, we established here the pathophysiological relationship between YY1 as well as sST2 and Dox-induced cardiotoxicity. Note that the endogenous silencing of *YY1* in hiPSCMs exposed to Dox prevented Dox-induced sST2 overexpression, which led to decreased CIC. In this setting, our data demonstrated the deleterious role of sST2 in Dox-induced cardiotoxicity. Thus, the exogenous addition of sST2, both in hiPSCMs and mice treated with *AM106* and exposed to Dox, was able to prevent the analyzed cardioprotective effects and was related to *AM106*. Perhaps most importantly, concomitant blocking of *miR-106b* and silencing of endogenous *PR55α* expression levels rescued the *miR-106b*-induced phenotype, supporting the notion that the PR55α regulatory subunit acted as a functional mediator of *miR-106b*.

In summary, it was demonstrated here that an increase in Dox-induced *miR-106b* was able to downregulate the PR55α subunit, which led to a decrease both in PP2A activity as well as an accumulation of the phosphorylated HDAC4 protein in cytosol. *AM106* treatment was able to prevent Dox-induced PR55α degradation, facilitate HDAC4 dephosphorylation by PP2A, and increase HDAC4-YY1 interaction, which led to decreased *sST2* expression and release by LV myocardium. Furthermore, we have been able to assess the role that the sST2 isoform plays in Dox-induced cardiotoxicity.

This study has several limitations, which should be pointed out. First, our conclusions are based on the use of a commercial antagomir sequence, which is not allowed to be used for human trials. The design and development of a similar oligonucleotide sequence are required for preclinical assays. In addition, our conclusions regarding the safety of *AM106* treatment are approximate. We need to generate the *AM106* sequence under GMP conditions to test its biosafety.

MATERIAL AND METHODS

hiPSCMs

hiPSCs were obtained from Phenocell (cat. no. PCi_CAU) and cultured according to the manufacturer's instructions. In brief, hiPSCs on a suitable matrix to allow attachment of cell aggregates (Matrigel) were grown to 80% confluence using mTeSR plus medium. In passage 20, we started the directed differentiation process using a standardized protocol in our laboratory. Thus, the culture medium was removed and changed to RPMI-1640 with a B27 supplement

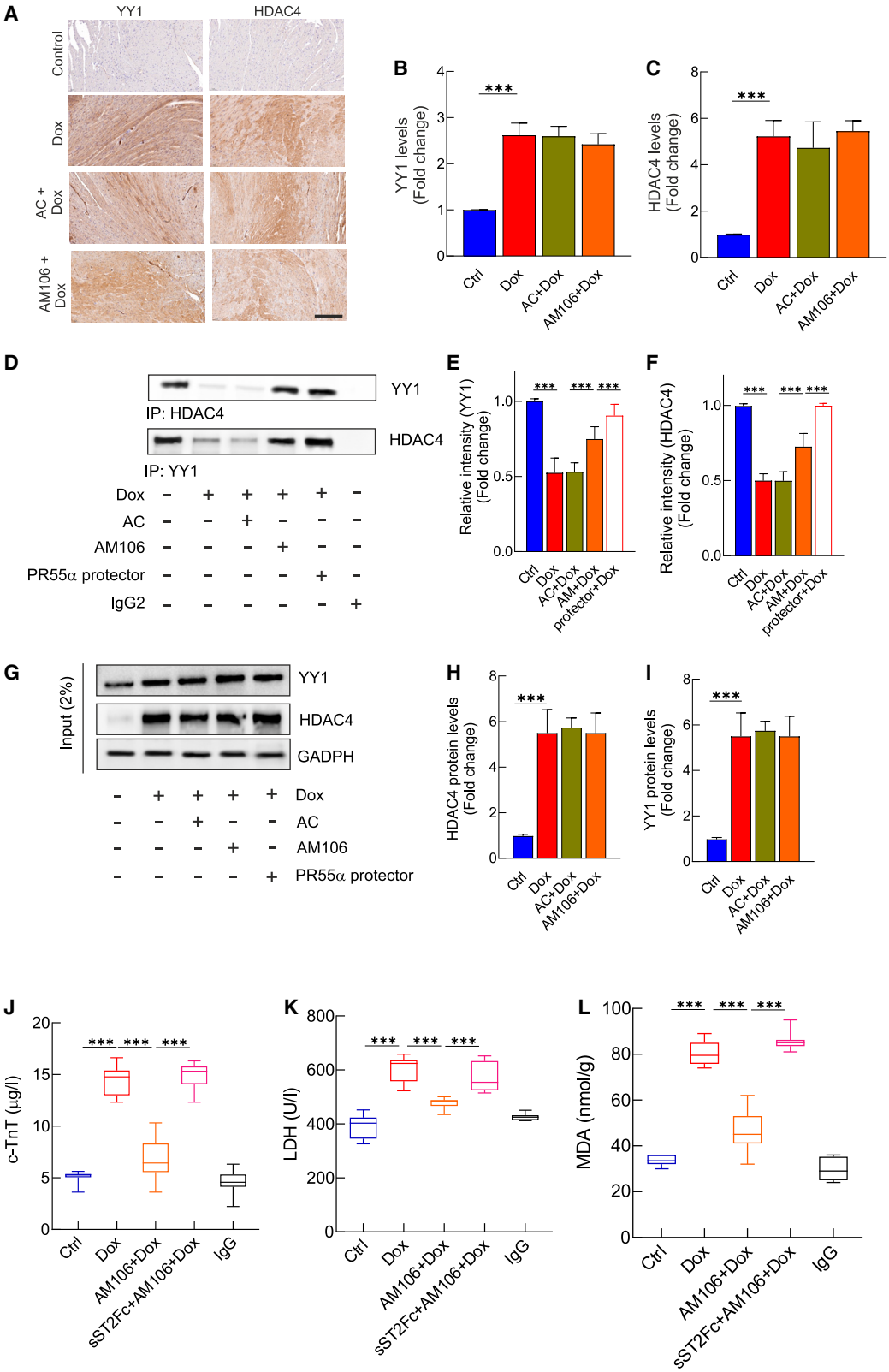

(legend on next page)

minus insulin (basal differentiation supplement) with 4 μM CHIR99021 (day 0). On day 3, the medium was changed to a basal differentiation supplement and 3 μM IWR-1. On day 5, the medium was refreshed with a basal differentiation supplement. The medium was changed on day 8 to RPMI-1640 with a B27 supplement (cited above as RMPI/B27). On day 11, the medium was changed to RPMI-1640 without glucose and with B27 minus insulin. On day 14, the medium was changed to RPMI/B27, a procedure that was repeated every 72 h. Cells in normoxia were maintained under normal culture conditions (5% CO_2 in a 37°C humidified incubator). Beating clusters were observed after 7–14 days. A standardizing gene expression profiling (qRT-PCR) of both hiPSCs as well as hiPSCMs was carried out in each human isolated clone before starting assays (Figure S13). Specific primer sequences are detailed in Table 2. The cardiotoxic treatment was carried out by exposing the cell culture to 5 μM Dox for different time periods unless otherwise mentioned. The Dox concentration was selected according to previous studies,[53] reproducing the plasma peak concentration reached by standard infusion in patients,[54] while 0.2 μM Dox is the concentration of Dox that lacks toxic effect and is used to reproduce the potential effect of the vehicle in which Dox is dissolved. In the fixed-time experiments, the incubation with Dox was set at 15 h as this is the time at which the effects are clearly visible and statistically significant. All *in vitro* assays were performed as three biological replicates, with technical replicates each time.

Transfection procedure

The *hsa-miR-106b-5p* sequence of nucleotides was obtained from www.MiRbase.org. Human *miR-106b* (accession no. MIMAT0000680) and the nucleotide sequence of 5′-UAAAGUGCUGACAGUGCAGAU-3′ are homologous between mice and humans. To express or block the specific *miR-106b* function, synthetic *antimiR-106* oligonucleotides were transfected into hiPSCM cells. Lipofectamine RNAiMAX transfection reagent (Thermo Fisher Scientific) was used according to the manufacturer's instructions. The miRCURY locked nucleic acid (LNA) miRNA Inhibitor (*AM106*, YCI0202832) (5′-CACTGTCAGCACTTT-3′) and the MiRCURY LNA miRNA Mimic (*106b mimic*, YM00471973) (5′-UAAAGUGCUGACAGUGCAGAU-3′), together with their respective controls (AC, YCI0200428; 5′-ACGTCTATACGCCCA-3′) (NC, YM00479903; 5′-GAUGGCAUUCGAUCAGUUCUA-3′), were purchased from QIAGEN (the sequences are shown without the LNA pattern). Two days before transfection, hiPSCM cells were seeded in six-well plates with 2 mL of STEMdiff Cardiomyocyte Support Medium (STEMCELL Technologies) to a density of 60%. Stock transfection mixes were made according to the manufacturer's instructions. In brief, 9 μL of Lipofectamine reagent was diluted in 141 μL of Opti-MEM I Medium (Invitrogen) and incubated for 5 min at room temperature (RT). In another tube, anti-miRNA or the specific control oligonucleotides were diluted with Opti-MEM to a final concentration of 50 nM. Both mixes were incubated together for 30 min at RT to allow complex formation between the miRNA and lipids. To transfect the cells, the STEMdiff Cardiomyocyte Support Medium was removed and replaced with 1.75 mL fresh medium and 250 μL of the appropriate transfection mix. The cells were incubated at 37°C for 48 days, after which hiPSCMs were treated with 5 μM Dox for 15 h under normal culture conditions, as described previously. The efficiency of *miR-106b* inhibition was tested in parallel using both hiPSCMs and LV myocardium from mice (Figure S1). The experimental procedure to silence endogenous *PR55α* or *YY1* mRNA levels in hiPSCMs was similar to that described above. Here, naive cells were washed and transfected with four interference RNA sequences specifically designed for human *PR55α* (5′-GAAAUUACAGACAGGAGUU-3′, 5′-UAUCAAGCCUGCCAAUAUG-3′, 5′-UAUGAUGACUAGAGACUAU-3′, and 5′-GCAGAUGAUUUGCGGAUUA-3′) or for the human *YY1* mRNA sequence (A-011796-16-0005, A-011796-17-0005, A-011796-18-0005, and A-011796-19-0005) or with non-targeting Accell siRNA sequences (*siCtrl*) (D-001810-10-05) siRNA. The transfection concentration was 25 nM, and the efficiency was determined and is shown in Figure S14. To block the specific *miR-106b-5p/PR55α* interaction, miRCURY LNA miRNA Power Target Site Blockers (QIAGEN) (*PR55α protector*) were used (50 nM; final concentration) (seed sequence to be masked: 5′-CACUUU-3′). When indicated, sST2-Fc or IgG (100 nM in both cases) were added 24 h before *AM106* treatment.

RNA isolation and qRT-PCR

Total RNA was isolated from hiPSCMs (2×10^6 cells) or the LV myocardium (20 mg). The RNA was purified with the RNeasy Mini Kit (QIAGEN), and the cDNA was prepared with the iScript cDNA Synthesis Kit (Bio-Rad Lab, Madrid) according to the manufacturer's recommendation. A qRT-PCR) was performed with TB Green Premix Ex Taq II (Tli RNase H Plus) Master Mix (Takara Bio, Europe). Glyceraldehyde 3-phosphate dehydrogenase (*GAPDH*) was used as the housekeeping gene. Sequences of the primers used (Merck) are listed in Table 2.

miRNA isolation and quantification assay

Total RNA was isolated from hiPSCMs (2×10^6 cells) or LV myocardium (30 mg) with the miRNeasy kit (QIAGEN) and reverse-transcribed to cDNA using the miRCURY LNA Universal RT microRNA cDNA synthesis kit (QIAGEN). Mature *miR-106b* expression levels were assessed by qRT-PCR using the miRCURY LNA UniRT PCR primer for *miR-106b-5p* (QIAGEN) and Power SYBR Green PCR Master Mix (Thermo Fisher Scientific). *U6* (QIAGEN) was used as an internal control to normalize *miR-106b* expression.

Assay for cell viability

After seeding 5×10^3 cells in each 96-well plate, they were incubated in 5% CO_2 at 37°C for 24 h. After the cited treatment, MTT solution

Figure 6. Anti-miR-106b treatment promotes nuclear interaction between HDAC4 and YY1

(A–C) Representative immunohistochemistry images (A), and analysis for YY1 (B) and HDAC4 (C). Scale bar, 100 μm. (D–I) Co-immunoprecipitation assays, representative western blots, and analysis. (J–L) Levels of c-TnT, LDH activity, and MDA levels. All quantifications are derived from n = 10 mice/group. All quantitative data are presented as mean ± SEM. ***$p < 0.001$ determined by one-way ANOVA followed by post hoc tests with Bonferroni correction. Abbreviations have been described previously.

Table 2. Primer sequences used for quantitative real-time PCR analysis

	Primer	Forward (5′–3′)	Reverse (5′–3′)
Mice	GAPDH	GTGAAGGTCGGTGTGAACG	TCGTTGATGGCAACAATCTC
	FOG2	GCTAGGACCTCTGGCTAATGTATC	ATGGTGTGTTCACTAGGCGG
	MNF2	GCTCCTGAAGGATGACCTCG-	CGTCTGCATCAGCGTGGACTC
	YY1	TGAGAAAGCATCTGCACACC	CGCAAATTGAAGTCCAGTGA
	VEGF	ATCTGCATGGTGATGTTGGA	GGGCAGAATCATCACGAAGT
Human	FOG2	CAAAGGAGGCTGAAGATGGC	CAAAGTGAGCCTCGATCAGC
	GAPDH	TCAACGACCACTTTGTCAAGCTCA	GCTGGTGGTCCAGGGGTCTTACT
	NANOG	CATGAGTGTGGATCCAGCTTG	CCTGAATAAGCAGATCCATGG
	NKX 2-5	CTACGGTTATAACGCCTACCC	CGAAGTTCACGAAGTTGTTGTT
	PR55α	CCCCGGTTCAGCCTCGGACT	ACGGATGCCCTCGGTGGCTA
	OCT4	TCTTTCCACCAGGCCCCCGGCTC	TGCGGGCGGACATGGGGAGATCC
	YY1	ACATCTGCACACCCACGGT	GCGTTTCCCACAGCCTTCG

(1 mg/mL) was added to each well, and incubation was performed for 1 h at 37°C. Next, the medium containing MTT was removed, and 100 μL of DMSO was added to each well and pipetted several times to form a completely uniform suspension. The solution was then shaken for 5 min at RT until formazan crystals were completely dissolved. The absorbance of the samples was read at 570 nm, and the background value at 690 nm was subtracted. The index of cell survival at each time point corresponds to the percentage with respect to the control.

Caspase assay

A caspase assay was performed as per the manufacturer's instructions with the Caspase-Glo 3/7 kit (Promega). In this setting, the hiPsCMs were treated with 5 μM Dox for 15 h. The hiPSCMs and caspase assay reagent were then left at RT for 30 min. The next step was adding an equal amount of caspase assay reagent and further incubating for 30 min at RT. Luminescence was measured using a microplate reader, CLARIOstar Plus (BMG Labtech).

Western blotting

The protein extracts (15 μg) obtained were denatured, separated by SDS-PAGE (Bio-Rad), transferred onto a PVDF membrane (Millipore), and probed with antibodies to glyceraldehyde 3-phosphate dehydrogenase (GAPDH) (Merck, 8795, 1:5,000), TATA binding protein (TBP) (Cell Signaling Technology, 8515, 1:1,000), PR55α (Cell Signaling Technology, 5689, 1:1,000), phospho-HDAC4 (Abcam, ab39408, 1:2,000), HDAC4 (Cell Signaling Technology, 5392, 1:1,000), YY1 (Cell Signaling Technology, 2185, 1:1,000), and sST2 (Proteintech, 11,920-1-AP, 1:1,000). Equal loading in the lanes was checked with the GAPDH or TBP antibodies; markers to the cytosol and nucleus fraction, respectively. Membranes were developed using HRP-conjugated secondary antibodies and a Pierce ECL western blotting substrate (Thermo Fisher Scientific). Signals were detected using chemiluminescence and quantified using ImageJ 1.44p pixel analysis (US National Institutes of Health). The methods are explained in more detail in the supplemental information.

Transfection of hiPsCMs with AAV6

The human PR55α Adenovirus (accession no. AAV-219651) *AAV6* and a control *AAV6-GFP* (cat. no. 7008) were obtained from Vector Biolabs. When indicated, *AAV6* was used at an MOI of 10^4 for human iPSCMs.

Animals and ethics statement

Seven- to 9-week-old C57Bl/6J male mice (weighing 25–30 g) were purchased from the ENVIGO Laboratory. The mice were housed in a specific pathogen-free environment with a relative humidity of 50% ± 5% at 23°C ± 2°C with 12 h light and dark cycles. The mice had free access to food and water. The study protocol was examined and approved by the Institutional Ethics and Animal Experimentation Committee of the University of Murcia according to Spanish Government Guidelines and European Community Guidelines for animal care (authorized no. A13220607). All methods were carried out following relevant guidelines and regulations.

Dox-induced cardiotoxicity: Animal model and treatments

A previously described mouse model of Dox-induced cardiotoxicity was used.[55] In the present study, C57BL/6J mice were given Dox at a dose of 5 mg/kg intraperitoneally weekly for 5 consecutive weeks (cumulative dose: 25 mg/kg) to achieve CIC. The animals were sacrificed after 8 weeks.

In vivo delivery of LNA-antimiR oligonucleotides and experimental design

To achieve a systemic loss of function of *miR-106b*, *AM106* (20 mg/kg) was intravenously (caudal vein) administered 7 days before the first Dox injection (5 mg/kg, i.p.). Previous studies have demonstrated that four consecutive injections of an LNA-antimiR were sufficient to inhibit a cardiac miRNA effect for at least 2 months.[11] The mice were injected for 5 consecutive weeks and, simultaneously, with 5 mg/kg Dox and 20 mg/kg *AM106* and sacrificed 8 weeks later (Figure 5A). The control animals and mice treated with Dox were then randomized into control or treated groups. The animals were

randomly divided into four experimental groups: (1) control mice receiving saline for 8 weeks, (2) mice treated with Dox receiving saline for 8 weeks, (3) mice treated with Dox receiving *antimiR-Ctrl* (*AC*) for 8 weeks, and (4) mice treated with Dox receiving *AM106* for 8 weeks. To investigate the effect of sST2-Fc, the mice received i.p. (caudal vein) injections of recombinant sST2-Fc at doses of 100 μg/mouse from the first *AM106* administration and then once every 3 days until sacrificed. The control mice received similar amounts of purified human IgG only.

LV structure and function

A trained and blinded investigator (M.J.F.d.P.) performed transthoracic echocardiographic examination in all mice before Dox treatment (baseline) and 8 weeks after Dox administration, under anesthesia (1%–1.5% isoflurane). A Vevo 3100 high-resolution ultrasound system (VisualSonics, Toronto, Canada) with a 30-MHz center-frequency transducer and an integrated rail system was used for image acquisition. The echocardiographic parameters determined in each examination were as follows: LV end-diastolic and end-systolic dimensions were measured by parasternal short-axis M-mode echocardiography, and FS was calculated using the Vevo program; end-systolic (LVESV) and end-diastolic (LVEDV) volumes and EF were calculated in 2D mode using the modified Simpson's method from the four-chamber long-axis view; pulsed Doppler parameters of mitral inflow, including early peak diastolic velocity (E), late peak diastolic velocity (A), and E/A ratio using the apical four-chamber view; pulsed Doppler tissue parameters at the mitral septal annulus, including peak systolic velocity (S′), early peak diastolic velocity (E′), late peak diastolic velocity (A′), and calculation of E/E′ ratio. All echocardiographic parameters were measured according to recommendations of the ESC Working Group on Myocardial Function in Adult Rodents.[56] Interpretation of echocardiographic measurements was blinded to the mice group.

Tissue samples and histology

Eight weeks after the first administration of Dox, the animals were sacrificed, and their hearts were arrested in diastole by intravenous injection of 0.2 mL of 30% (w/v) potassium chloride (Merck). The hearts were excised and rinsed with ice-cold DPBS before the removal of the right ventricle and the atria. For the histopathological analyses, mid-papillary slices of the left ventricle of seven mice from each treatment group were fixed in 4% (w/v) formaldehyde for up to 24 h before paraffin embedding. FITC-labeled wheat germ agglutinin (WGA, Life Technologies, 1:200 dilution) staining was performed to detect the cardiomyocyte cross-sectional area.[11] The cardiac myocyte membranes were observed using fluorescence microscopy. The morphometric analyses were performed using Image-Pro Plus software. Only cells with well-defined cell membranes were selected. At least 100 myocytes were analyzed in each group. Sirius red staining was performed to evaluate fibrosis. For its quantification, at least six random pictures were taken from each slide at 20× magnification. Collagen deposition (red) was used to define fibrosis, which is expressed as the percentage of red pixels to green pixels quantitated using Digital Image Hub software version 4.0.6. Specifically, to evaluate angiogenesis, CD31 levels were tested in the cited formalin-fixed paraffin-embedded tissues. In brief, after deparaffination and rehydration a demasking antigen procedure was performed using a commercial solution (high pH demasking antigen solution, Agilent-Dako Technologies, Madrid, Spain). Endogenous peroxidase was then blocked (peroxidase blocking, Agilent-Dako) followed by overnight incubation with the primary antibody (polyclonal rabbit anti-CD31 antigen [Abcam, Oxford, UK]). On the second day, sections were incubated with a secondary HRP-labeled polymer system (ImmPRESS anti-rabbit detection kit, Vector Laboratories, Burlingame), and revealed with 2-2′diaminobencidine and hematoxylin counterstaining. The positive immunoreaction was identified by a dark-brown precipitate with a membrane/cytoplasm pattern within vessels. To determine the surface of CD31-positive immunolabeling, all sections were X400 digitalized (Pannoramic MIDI-II digital slide scanner, 3D Histech, Budapest, Hungary). Ten random high-power fields (×400) were obtained from each section and analyzed using specialized digital analysis software (ImageJ, v.1.53t, NIH). The final result reflects the percentage of positive-CD31 surface with respect to the surface of the whole field (60,900 μm^2). For other molecular-cellular biological studies, tissue from the LV myocardium was collected and stored at − 80°C for RNA extraction and western blot. The observers who performed the image analyses and the molecular and cellular biological experiments were blinded to the experimental groups.

Immunohistochemistry

The next experimental procedure was performed as described previously, with some modifications.[10] In brief, the sections (3 μm) from paraffin-embedded mid-papillary slices of LV myocardium were placed on poly-L-lysine-coated glass slides. The sections were then de-paraffinized and pre-treated in DAKO PT Link for 20 min at 97°C. For YY1 or HDAC4 staining, the rehydrated sections were incubated overnight with a polyclonal YY1 antibody (working dilution 1:500, Proteintech, Chicago, IL) or with a polyclonal HDAC4 antibody (working dilution 1:500, Proteintech). The sections were then incubated with anti-rabbit biotinylated-labeled polymer (Dako EnVision) according to the manufacturer's instructions and revealed with 2,2′-diaminobencidine. A cytoplasmic dark-brown precipitate indicated positive immunostaining. The images were captured using a Zeiss Axioscope A10 microscope (Carl Zeiss, Madrid, Spain). Six random pictures were taken of each slide at 10× magnification (n = 7 slices/each treated group).

Statistical analysis

The data obtained were reported as mean ± SEM. Statistical differences were evaluated by fitting linear models with interactions determined by one-way ANOVA followed by post hoc tests with Bonferroni correction. A p value <0.05 was considered significant.

DATA AVAILABILITY

The data that support the findings of this study are available from the corresponding author upon reasonable request.

SUPPLEMENTAL INFORMATION

Supplemental information can be found online at https://XX

ACKNOWLEDGMENTS

This study was supported by a grant from the Instituto de Salud Carlos III (PI19/00519). A.L. is a Ramon and Cajal Researcher in the Department of Medicine, University of Murcia (RYC2019-027635-I; supported by MCIN/AEI/10.13039/501100011033 and by FSE for the future) and M.d.C.A.-L. is a Juan de la Cierva Researcher in the Hematovascular Pathophysiology laboratory, Spanish National Center for Cardiovascular Research (FJC2020-042841-I).

AUTHOR CONTRIBUTIONS

M.d.C.A.-L. and A.L. conceived the work, generated the experimental data, and wrote and edited the manuscript. A.L. is the guarantor of this work and, as such, had full access to all the data in the study and takes responsibility for the integrity of the data and the accuracy of the analysis. Echocardiographic measurements were carried out by M.J.F.d.P. and S.P.-O. J.J.F. helped with the analysis and contributed to writing the discussion. D.P.-F. and F.S. helped with the analysis, contributed to writing the discussion, and edited the manuscript. M.R.B. tested the AM106 biodistribution and toxicity assays.

DECLARATION OF INTERESTS

The authors declare no competing interests.

REFERENCES

1. Hwang, T.J., Kesselheim, A.S., and Gyawali, B. (2018). Affordability and price increases of new cancer drugs in clinical guidelines, 2007-2016. JNCI Cancer Spectr. *2*, pky016.
2. Zamorano, J.L., Lancellotti, P., Rodriguez Muñoz, D., Aboyans, V., Asteggiano, R., Galderisi, M., Habib, G., Lenihan, D.J., Lip, G.Y.H., Lyon, A.R., et al. (2016). 2016 ESC Position Paper on cancer treatments and cardiovascular toxicity developed under the auspices of the ESC Committee for Practice Guidelines: the Task Force for cancer treatments and cardiovascular toxicity of the European Society of Cardiology (ESC). Eur. Heart J. *37*, 2768–2801.
3. Cardinale, D., Iacopo, F., and Cipolla, C.M. (2020). Cardiotoxicity of anthracyclines. Front. Cardiovasc. Med. *7*, 26.
4. Henriksen, P.A. (2018). Anthracycline cardiotoxicity: an update on mechanisms, monitoring and prevention. Heart *104*, 971–977.
5. Menna, P., Paz, O.G., Chello, M., Covino, E., Salvatorelli, E., and Minotti, G. (2012). Anthracycline cardiotoxicity. Expert Opin. Drug Saf. *11* (*Suppl 1*), S21–S36.
6. Agunbiade, T.A., Zaghlol, R.Y., and Barac, A. (2019). Heart failure in relation to anthracyclines and other chemotherapies. Methodist Debakey Cardiovasc. J. *15*, 243–249.
7. Yancy, C.W., Jessup, M., Bozkurt, B., Butler, J., Casey, D.E., Colvin, M.M., Drazner, M.H., Filippatos, G.S., Fonarow, G.C., Givertz, M.M., et al. (2017). 2017 ACC/AHA/HFSA focused update of the 2013 ACCF/AHA guideline for the management of heart failure: a report of the American College of Cardiology/American heart association task force on clinical practice guidelines and the heart failure society of America. J. Card. Fail. *23*, 628–651.
8. Bosch, X., Rovira, M., Sitges, M., Domènech, A., Ortiz-Pérez, J.T., De Caralt, T.M., Morales-Ruiz, M., Perea, R.J., Monzó, M., and Esteve, J. (2013). Enalapril and carvedilol for preventing chemotherapy-induced left ventricular systolic dysfunction in patients with malignant hemopathies: the OVERCOME trial (preventiOn of left Ventricular dysfunction with Enalapril and caRvedilol in patients submitted to intensive ChemOtherapy for the treatment of Malignant hEmopathies). J. Am. Coll. Cardiol. *61*, 2355–2362.
9. Gulati, G., Heck, S.L., Ree, A.H., Hoffmann, P., Schulz-Menger, J., Fagerland, M.W., Gravdehaug, B., Von Knobelsdorff-Brenkenhoff, F., Bratland, Å., Storås, T.H., et al. (2016). Prevention of cardiac dysfunction during adjuvant breast cancer therapy (PRADA): a 2 × 2 factorial, randomized, placebo-controlled, double-blind clinical trial of candesartan and metoprolol. Eur. Heart J. *37*, 1671–1680.
10. Asensio-Lopez, M.C., Lax, A., Fernandez del Palacio, M.J., Sassi, Y., Hajjar, R.J., Januzzi, J.L., Bayes-Genis, A., and Pascual-Figal, D.A. (2019). Yin-Yang 1 transcription factor modulates ST2 expression during adverse cardiac remodeling post-myocardial infarction. J. Mol. Cell. Cardiol. *130*, 216–233.
11. Hohl, M., Wagner, M., Reil, J.C., Müller, S.A., Tauchnitz, M., Zimmer, A.M., Lehmann, L.H., Thiel, G., Böhm, M., Backs, J., and Maack, C. (2013). HDAC4 controls histone methylation in response to elevated cardiac load. J. Clin. Invest. *123*, 1359–1370.
12. Kreusser, M.M., and Backs, J. (2014). Integrated mechanisms of CaMKII-dependent ventricular remodeling. Front. Pharmacol. *5*, 36.
13. Chen, L., Heikkinen, L., Wang, C., Yang, Y., Sun, H., and Wong, G. (2019). Trends in the development of miRNA bioinformatics tools. Brief. Bioinform. *20*, 1836–1852.
14. Nunes, D.N., Dias-Neto, E., Cardó-Vila, M., Edwards, J.K., Dobroff, A.S., Giordano, R.J., Mandelin, J., Brentani, H.P., Hasselgren, C., Yao, V.J., et al. (2015). Synchronous down-modulation of miR-17 family members is an early causative event in the retinal angiogenic switch. Proc. Natl. Acad. Sci. USA *112*, 3770–3775.
15. Zhang, Z., Ursin, R., Mahapatra, S., and Gallicano, G.I. (2018). CRISPR/CAS9 ablation of individual miRNAs from a miRNA family reveals their individual efficacies for regulating cardiac differentiation. Mech. Dev. *150*, 10–20.
16. Ventura, A., Young, A.G., Winslow, M.M., Lintault, L., Meissner, A., Erkeland, S.J., Newman, J., Bronson, R.T., Crowley, D., Stone, J.R., et al. (2008). Targeted deletion reveals essential and overlapping functions of the miR-17 through 92 family of miRNA clusters. Cell *132*, 875–886.
17. Raso, A., Dirkx, E., Sampaio-Pinto, V., el Azzouzi, H., Cubero, R.J., Sorensen, D.W., Ottaviani, L., Olieslagers, S., Huibers, M.M., de Weger, R., et al. (2022). Author Correction: a microRNA program regulates the balance between cardiomyocyte hyperplasia and hypertrophy and stimulates cardiac regeneration. Nat. Commun. *13*, 4977.
18. Chiang, D.Y., Kongchan, N., Beavers, D.L., Alsina, K.M., Voigt, N., Neilson, J.R., Jakob, H., Martin, J.F., Dobrev, D., Wehrens, X.H.T., and Li, N. (2014). Loss of microRNA-106b-25 cluster promotes atrial fibrillation by enhancing ryanodine receptor type-2 expression and calcium release. Circ. Arrhythm. Electrophysiol. *7*, 1214–1222.
19. Li, P., Shen, M., Gao, F., Wu, J., Zhang, J., Teng, F., and Zhang, C. (2017). An antagomir to MicroRNA-106b-5p ameliorates cerebral ischemia and reperfusion injury in rats via inhibiting apoptosis and oxidative stress. Mol. Neurobiol. *54*, 2901–2921.
20. Matilla, L., Ibarrola, J., Arrieta, V., Garcia-Peña, A., Martinez-Martinez, E., Sádaba, R., Alvarez, V., Navarro, A., Fernández-Celis, A., Gainza, A., et al. (2019). Soluble ST2 promotes oxidative stress and inflammation in cardiac fibroblasts: an in vitro and in vivo study in aortic stenosis. Clin. Sci. *133*, 1537–1548.
21. Rodriguez-Outeiriño, L., Hernandez-Torres, F., Ramirez de Acuña, F., Rastrojo, A., Creus, C., Carvajal, A., Salmeron, L., Montolio, M., Soblechero-Martin, P., Arechavala-Gomeza, V., et al. (2022). miR-106b is a novel target to promote muscle regeneration and restore satellite stem cell function in injured Duchenne dystrophic muscle. Mol. Ther. Nucleic Acids *29*, 769–786.
22. Yu, L.X., Zhang, B.L., Yang, M.Y., Liu, H., Xiao, C.H., Zhang, S.G., and Liu, R. (2019). MicroRNA-106b-5p promotes hepatocellular carcinoma development via modulating FOG2. OncoTargets Ther. *12*, 5639–5647.
23. Paroni, G., Cernotta, N., Dello Russo, C., Gallinari, P., Pallaoro, M., Foti, C., Talamo, F., Orsatti, L., Steinkühler, C., and Brancolini, C. (2008). PP2A regulates HDAC4 nuclear import. Mol. Biol. Cell *19*, 655–667.
24. Shimizu, E., Nakatani, T., He, Z., and Partridge, N.C. (2014). Parathyroid hormone regulates histone deacetylase (HDAC) 4 through protein kinase A-mediated phosphorylation and dephosphorylation in osteoblastic cells. J. Biol. Chem. *289*, 21340–21350.

25. Lipshultz, S.E., Colan, S.D., Gelber, R.D., Perez-Atayde, A.R., Sallan, S.E., and Sanders, S.P. (1991). Late cardiac effects of doxorubicin therapy for acute lymphoblastic leukemia in childhood. N. Engl. J. Med. *324*, 808–815.

26. Asensio-López, M.C., Lax, A., Pascual-Figal, D.A., Valdés, M., and Sánchez-Más, J. (2011). Metformin protects against doxorubicin-induced cardiotoxicity: involvement of the adiponectin cardiac system. Free Radic. Biol. Med. *51*, 1861–1871.

27. Castets, P., Rion, N., Théodore, M., Falcetta, D., Lin, S., Reischl, M., Wild, F., Guérard, L., Eickhorst, C., Brockhoff, M., et al. (2019). mTORC1 and PKB/Akt control the muscle response to denervation by regulating autophagy and HDAC4. Nat. Commun. *10*, 3187.

28. Duval, A.P., Jeanneret, C., Santoro, T., and Dormond, O. (2018). mTOR and tumor cachexia. Int. J. Mol. Sci. *19*, 2225.

29. Miller, K.D., Nogueira, L., Mariotto, A.B., Rowland, J.H., Yabroff, K.R., Alfano, C.M., Jemal, A., Kramer, J.L., and Siegel, R.L. (2019). Cancer treatment and survivorship statistics, 2019. CA. Cancer J. Clin. *69*, 363–385.

30. Van Rooij, E., Marshall, W.S., and Olson, E.N. (2008). Toward microRNA-based therapeutics for heart disease: the sense in antisense. Circ. Res. *103*, 919–928.

31. van Rooij, E., and Kauppinen, S. (2014). Development of microRNA therapeutics is coming of age. EMBO Mol. Med. *6*, 851–864.

32. Nouraee, N., and Mowla, S.J. (2015). miRNA therapeutics in cardiovascular diseases: promises and problems. Front. Genet. *6*, 232.

33. Li, N., Liu, Y., Miao, Y., Zhao, L., Zhou, H., and Jia, L. (2016). MicroRNA-106b targets FUT6 to promote cell migration, invasion, and proliferation in human breast cancer. IUBMB Life *68*, 764–775.

34. Wei, K., Pan, C., Yao, G., Liu, B., Ma, T., Xia, Y., Jiang, W., Chen, L., and Chen, Y. (2017). MiR-106b-5p promotes proliferation and inhibits apoptosis by regulating BTG3 in non-small cell lung cancer. Cell. Physiol. Biochem. *44*, 1545–1558.

35. Liu, F., Gong, J., Huang, W., Wang, Z., Wang, M., Yang, J., Wu, C., Wu, Z., and Han, B. (2014). MicroRNA-106b-5p boosts glioma tumorigensis by targeting multiple tumor suppressor genes. Oncogene *33*, 4813–4822.

36. Asensio-López, M.C., Sánchez-Más, J., Pascual-Figal, D.A., Abenza, S., Pérez-Martínez, M.T., Valdés, M., and Lax, A. (2013). Involvement of ferritin heavy chain in the preventive effect of metformin against doxorubicin-induced cardiotoxicity. Free Radic. Biol. Med. *57*, 188–200.

37. Li, Z., Li, H., Liu, B., Luo, J., Qin, X., Gong, M., Shi, B., and Wei, Y. (2020). Inhibition of miR-25 attenuates doxorubicin-induced apoptosis, reactive oxygen species production and DNA damage by targeting PTEN. Int. J. Med. Sci. *17*, 1415–1427.

38. Chan, B.Y.H., Roczkowsky, A., Cho, W.J., Poirier, M., Sergi, C., Keschrumrus, V., Churko, J.M., Granzier, H., and Schulz, R. (2021). MMP inhibitors attenuate doxorubicin cardiotoxicity by preventing intracellular and extracellular matrix remodelling. Cardiovasc. Res. *117*, 188–200.

39. Guan, X., Wang, L., Liu, Z., Guo, X., Jiang, Y., Lu, Y., Peng, Y., Liu, T., Yang, B., Shan, H., et al. (2016). miR-106a promotes cardiac hypertrophy by targeting mitofusin 2. J. Mol. Cell. Cardiol. *99*, 207–217.

40. Gallicano, G.I., Fu, J., Mahapatra, S., Sharma, M.V.R., Dillon, C., Deng, C., and Zahid, M. (2022). Reversing cardiac hypertrophy at the source using a cardiac targeting peptide linked to miRNA106a: targeting genes that cause cardiac hypertrophy. Pharmaceuticals *15*, 871.

41. Ding, M., Shi, R., Cheng, S., Li, M., De, D., Liu, C., Gu, X., Li, J., Zhang, S., Jia, M., et al. (2022). Mfn2-mediated mitochondrial fusion alleviates doxorubicin-induced cardiotoxicity with enhancing its anticancer activity through metabolic switch. Redox Biol. *52*, 102311.

42. Duan, J., Liu, X., Shen, S., Tan, X., Wang, Y., Wang, L., Kang, L., Wang, K., Wei, Z., Qi, Y., et al. (2023). Trophoblast stem-cell-derived exosomes alleviate cardiotoxicity of doxorubicin via improving Mfn2-mediated mitochondrial fusion. Cardiovasc. Toxicol. *23*, 23–31.

43. Jordan, J.H., Castellino, S.M., Meléndez, G.C., Klepin, H.D., Ellis, L.R., Lamar, Z., Vasu, S., Kitzman, D.W., Ntim, W.O., Brubaker, P.H., et al. (2018). Left ventricular mass change after anthracycline chemotherapy. Circ. Heart Fail. *11*, e004560.

44. Willis, M.S., Parry, T.L., Brown, D.I., Mota, R.I., Huang, W., Beak, J.Y., Sola, M., Zhou, C., Hicks, S.T., Caughey, M.C., et al. (2019). Doxorubicin exposure causes subacute cardiac atrophy dependent on the striated muscle-specific ubiquitin ligase MuRF1. Circ. Heart Fail. *12*, e005234.

45. Xia, P., Chen, J., Liu, Y., Fletcher, M., Jensen, B.C., and Cheng, Z. (2020). Doxorubicin induces cardiomyocyte apoptosis and atrophy through cyclin-dependent kinase 2-mediated activation of forkhead box O1. J. Biol. Chem. *295*, 4265–4276.

46. Hein, A.L., Seshacharyulu, P., Rachagani, S., Sheinin, Y.M., Ouellette, M.M., Ponnusamy, M.P., Mumby, M.C., Batra, S.K., and Yan, Y. (2016). PR55α subunit of protein phosphatase 2A supports the tumorigenic and metastatic potential of pancreatic cancer cells by sustaining hyperactive oncogenic signaling. Cancer Res. *76*, 2243–2253.

47. Khew-Goodall, Y., and Hemmings, B.A. (1988). Tissue-specific expression of mRNAs encoding alpha- and beta-catalytic subunits of protein phosphatase 2A. FEBS Lett. *238*, 265–268.

48. Silverstein, A.M., Barrow, C.A., Davis, A.J., and Mumby, M.C. (2002). Actions of PP2A on the MAP kinase pathway and apoptosis are mediated by distinct regulatory subunits. Proc. Natl. Acad. Sci. USA *99*, 4221–4226.

49. Letourneux, C., Rocher, G., and Porteu, F. (2006). B56-containing PP2A dephosphorylate ERK and their activity is controlled by the early gene IEX-1 and ERK. EMBO J. *25*, 727–738.

50. Herzig, S., and Neumann, J. (2000). Effects of serine/threonine protein phosphatases on ion channels in excitable membranes. Physiol. Rev. *80*, 173–210.

51. Lei, M., Wang, X., Ke, Y., and Solaro, R.J. (2015). Regulation of Ca(2+) transient by PP2A in normal and failing heart. Front. Physiol. *6*, 13.

52. Mazhar, S., Taylor, S.E., Sangodkar, J., and Narla, G. (2019). Targeting PP2A in cancer: combination therapies. Biochim. Biophys. Acta. Mol. Cell Res. *1866*, 51–63.

53. Asensio-Lopez, M.C., Sanchez-Mas, J., Pascual-Figal, D.A., De Torre, C., Valdes, M., and Lax, A. (2014). Ferritin heavy chain as main mediator of preventive effect of metformin against mitochondrial damage induced by doxorubicin in cardiomyocytes. Free Radic. Biol. Med. *67*, 19–29.

54. Gianni, L., Viganò, L., Locatelli, A., Capri, G., Giani, A., Tarenzi, E., and Bonadonna, G. (1997). Human pharmacokinetic characterization and in vitro study of the interaction between doxorubicin and paclitaxel in patients with breast cancer. J. Clin. Oncol. *15*, 1906–1915.

55. Gupta, S.K., Garg, A., Avramopoulos, P., Engelhardt, S., Streckfuss-Bömeke, K., Batkai, S., and Thum, T. (2019). miR-212/132 cluster modulation prevents doxorubicin-mediated atrophy and cardiotoxicity. Mol. Ther. *27*, 17–28.

56. Zacchigna, S., Paldino, A., Falcão-Pires, I., Daskalopoulos, E.P., Dal Ferro, M., Vodret, S., Lesizza, P., Cannatà, A., Miranda-Silva, D., Lourenço, A.P., et al. (2021). Towards standardization of echocardiography for the evaluation of left ventricular function in adult rodents: a position paper of the ESC Working Group on Myocardial Function. Cardiovasc. Res. *117*, 43–59.